Quantification and Exploration of Diurnal Oscillations in Tropical Cyclones

JOHN A. KNAFF

NOAA/Center for Satellite Applications and Research, Fort Collins, Colorado

CHRISTOPHER J. SLOCUM AND KATE D. MUSGRAVE

Cooperative Institute for Research in the Atmosphere, Colorado State University, Fort Collins, Colorado

(Manuscript received 24 October 2018, in final form 3 March 2019)

ABSTRACT

Diurnal oscillations of infrared cloud-top brightness temperatures (Tbs) in tropical cyclones (TCs) as inferred from storm-centered, direction-relative longwave infrared (~11 μm) imagery are quantified for Northern Hemisphere TCs (2005–15) using statistical methods. These methods show that 45%, 54%, and 61% of at least tropical storm-, hurricane-, and major hurricane-strength TC cases have moderate or strong diurnal signals. Principal component analysis–based average behavior of all TCs with intensities of 34 kt (17.5 m s^{-1}) or greater is shown to have a nearly symmetric diurnal signal where Tbs oscillate from warm to cold and cold to warm within and outside of a radius of approximately 220 km, with maximum central cooling occurring in the early morning (0300–0800 local standard time), and a nearly simultaneous maximum warming occurring near the 500-km radius—a radial standing wave with a node near 220-km radius. Amplitude and phase of these diurnal oscillations are quantified for individual 24-h periods (or cases) relative to the mean oscillation. Details of the diurnal behavior of TCs are used to examine preferred storm and environmental characteristics using a combination of spatial, composite, and regression analyses. Results suggest that diurnal, cloud-top Tb oscillations in TCs are strongest and most regular when storm characteristics (e.g., intensity and motion) and environmental conditions (e.g., vertical wind shear and low-level temperature advection) support azimuthally symmetric storm structures and when surrounding mid- and upper-level relative humidity values are greater. Finally, it is hypothesized that larger mid- and upper-level relative humidity values are necessary ingredients for robust, large-amplitude, and regular diurnal oscillations of Tbs in TCs.

1. Introduction

Early studies of cloud cover and rainfall over the tropical ocean and on tropical islands identified diurnal oscillations within these fields that results from the variability of convection throughout the day (Riehl 1947; Brier and Simpson 1969; Gray and Jacobson 1977; Weickmann et al. 1977). In addition to the influence of the semidiurnal atmospheric thermal tide, these studies note that the size of the island alters cloud cover and rainfall throughout the day—a finding that points to differences between the convection over the open ocean and convection affected by daytime, overland heating. In investigating prominent diurnal pulsing in the intertropical convergence zone using sounding arrays, Ciesielski et al. (2018) discuss the challenges that remain when attempting to quantify the diurnal cycle over the open ocean. Despite being restricted to a limited dataset, a field campaign, or a modeling framework, many studies of the diurnal cycle in the tropical atmosphere point to four physical mechanisms for modulating tropical deep convection—Nicholls (2015) includes an extensive review of the diurnal cycle mechanisms in the context of tropical cyclogenesis. The ''convergence/differential heating'' mechanism proposed by Gray and Jacobson (1977) and expanded to the tropical cyclone (TC) by McBride and Gray (1980) suggests that subsidence is enhanced in areas around deep convection at night through radiative cooling. As a result, low-level convergence is increased and leads to a pulse in convection in the early morning hours. As a second mechanism, Dudhia (1989), Miller and Frank (1993), and Tao et al. (1996) allude to large-scale radiative cooling playing a larger role in enhancing rainfall as the environmental relative humidity increases overnight. The third mechanism is referred to as the ''direct radiative–convective interaction'' or the lapse-rate mechanism (Kraus 1963; Randall et al. 1991; Xu and Randall 1995). In this

Corresponding author: John Knaff, john.knaff@noaa.gov

DOI: 10.1175/MWR-D-18-0379.1

mechanism, daytime shortwave radiation at cloud top suppresses convection by stabilizing the column. At night, longwave cooling at cloud top destabilizes the column by increasing the lapse rates allowing for deeper convection and increased rainfall. Hobgood (1986) surmised that this mechanism combined with that proposed by Gray and Jacobson (1977) produces diurnal oscillations in TCs. The final mechanism associates diurnal pulses of convection with the ''remote influences of continents'' (Silva Dias et al. 1987)—a mechanism that may explain some spatial discrepancies observed in over-ocean diurnal oscillations.

In tropical cyclones, the diurnal oscillation is typically described as manifesting itself through enhanced deep convection near the eyewall; later in the cycle, the cirrus canopy expands—the linkage between these two events is still not completely understood. The first iteration of this conceptual model in the literature appears in an early television-infrared imager study by Merritt and Wexler (1967), where the authors note that the canopy expands from noon to the late afternoon provided that the inner-core convection remains robust. Browner et al. (1977), Muramatsu (1983), Lajoie and Butterworth (1984), and Steranka et al. (1984) refine understanding of the nature of the cycle using brightness temperature (Tb) thresholds and split-window differences with infrared (IR) imagery. While this body of literature shares similar overarching findings that tropical cyclones exhibit diurnal oscillations in several meteorological fields, the individual studies reach different conclusions regarding the phase and amplitude of the oscillation. It is likely that these discrepancies arise from small sample sizes, the stage of the tropical cyclone life cycle (e.g., genesis, rapid intensification, quasi-steady state), meteorological variable (e.g., a metric for deep convection, circus canopy extent), dataset and threshold used, or the influence of the semidiurnal atmospheric thermal tide as postulated by Kossin (2002). In recent examinations of the diurnal oscillation, a more thorough version of the daily procession for convection in mature TCs has emerged. Dunion et al. (2014, hereafter D14) focus on evaluating IR data for cases with weak environmental deep-layer shear in the tropical North Atlantic that reach intensities at or greater than category 2 ($\geq$43 m s^{-1}) on the Saffir–Simpson hurricane wind scale. In Table 2 of D14,[1] the authors outline the progression of the diurnal pulse of the cirrus canopy in mature tropical cyclones based on 6-h differences in Tbs—the peak IR cooling associated with the diurnal pulse passes a radius of 200 km between 0400 and 0800 local standard time (LST) and a radius of 600 km between 1600 and 2000 LST; the peak IR warming associated with the minimum in deep convection passes a radius of 200 km between 2000 and 0000 LST and a radius of 600 km between 0200 and 0600 LST. The D14 diurnal clock mirrors the cycle described by Muramatsu (1983) for mature typhoons and the pattern documented in other types of tropical convection (see Ciesielski et al. 2018).

Kossin (2002), Bowman and Fowler (2015), and Leppert and Cecil (2016) note that the diurnal cycle is either not evident in some TC cases or that the signal does not follow the pattern outlined in prior work. In fact, Kossin (2002) states that few storms in his study have a strong diurnal signal in the deep-convective region within 200 km of the center using IR data. Through analyzing TRMM data to examine inner-core and rainband region convection, Bowman and Fowler (2015) and Leppert and Cecil (2016) also find that not all TCs exhibit a diurnal signal and that the diurnal signal is often entangled with the semidiurnal tide—findings that are consistent with Kossin (2002). These findings may appear to conflict with the D14 clock and suggest a gap in understanding diurnal oscillations in tropical cyclones. But, it is worth noting that the disconnects likely arise from region and field of interest (e.g., deep-convection in the inner-core region, canopy extent in the rainband region). Unfortunately, most numerical modeling studies on this subject have concentrated primarily on two topics: producing diurnal oscillations in modeled TCs and exploring the aforementioned physical mechanisms that may be responsible for diurnal oscillation of deep convection in TCs rather than the interplay between phase and amplitude of diurnal oscillations, storm characteristics, and storm large-scale environment. We will make comments on the latter when we summarize and discuss our results.

Given the ubiquity of the physical mechanisms associated with diurnal oscillations in the tropical atmosphere (e.g., Yang and Slingo 2001; Ciesielski et al. 2018), we are interested in understanding why the discrepancies in the TC literature exist by examining the global frequency of the presence of diurnal oscillations in tropical cyclones, the types of storm environments that diurnal oscillations would be expected, and storm/environment combinations that display robust diurnal oscillations. In section 2, we outline our datasets that consist of a satellite IR archive as well as storm and environmental parameters. Section 3 details our methods and findings resulting from quantifying the diurnal oscillations

[1] We note that the time ranges and radii listed in Table 2 of D14 are for the ''diurnal pulse passage'' of the cirrus canopy warming and cooling as defined by 6-h differences in Tbs while the schematic of the 24-h conceptual clock presented in Fig. 10 of D14 denotes the ''arrival time of the TC diurnal pulse.''

in the IR data, examining the tropical cyclone environment in our stratification of the types of diurnal oscillations found in tropical cyclones, evaluating a regression analysis of the environment, and applying our findings to two out-of-sample storms from the 2018 North Pacific tropical cyclone season. In section 4, we will discuss implications of our results.

2. Data

Northern Hemisphere, storm-centered, geostationary-satellite IR imagery, TC best track files, and large-scale environmental diagnostics are the primary datasets used in this study.

To help quantify the diurnal variations of deep convection associated with Northern Hemisphere TCs, we use IR satellite imagery over the period from 2005 to 2015 from an archive maintained at the NOAA Regional and Mesoscale Meteorology Branch that is collocated with the Cooperative Institute for Research in the Atmosphere (CIRA) at Colorado State University. The archive has navigated digital IR Tb images with central wavelengths near 11 μm that have been remapped to a common 4 km $\times$ 4 km resolution Mercator projection from the global constellation of geostationary satellites. For each TC in the dataset, the archive contains images at approximately 30-min temporal resolutions. For this analysis, 730 TCs are considered with 641 ultimately used. Exclusion of TCs from the analysis was done based IR imagery availability or best track intensity constraints discussed in section 3. The resulting dataset thus considers 77 323 unique images, resulting in 13 145 24-h periods (cases), many with overlapping time periods (0–24, 6–30 h, etc.), that are used for spatial, composite, and regression analysis as described in section 3. For the remainder of this paper, we refer to the dataset as the CIRA IR archive—Mueller et al. (2006), Zehr and Knaff (2007), and Knaff et al. (2014) provide additional details of the CIRA IR archive. In the context of diurnal and semidiurnal oscillations, Kossin (2002) used an earlier version of the CIRA IR archive to examine difference between the deep convective regions and the cirrus canopy.

Estimates of storm location and intensity are provided by the tropical cyclone best track database files of the Automated Tropical Cyclone Forecast (Sampson and Schrader 2000) system. This dataset amalgamates information generated by the National Hurricane Center, the Central Pacific Hurricane Center, and the Joint Typhoon Warning Center at six-hour intervals. It is important to note that these operational TC centers use the same 1-min maximum wind conventions for intensity estimation. However, since the subjective classification of tropical depression varies among basins and forecast centers, TCs with intensities less than 34 kt (17.5 m s^{-1}) are not considered in our analysis. For this work, we use cubic-spline interpolation to calculate position and intensity data as a function of time from the six-hour data in the best track files.

To assess the mean environment of tropical cyclones, we leverage the large-scale diagnostics calculated from operational numerical model output for the purposes of developing statistical–dynamical forecast models of intensity (DeMaria 2009; DeMaria et al. 2005; Kaplan et al. 2015), and wind radii (Knaff et al. 2017). A description of the Statistical Hurricane Intensity Prediction Scheme (SHIPS) Developmental Dataset is available on line at http://rammb.cira.colostate.edu/research/tropical_cyclones/ships/developmental_data.asp — the dataset and description are updated annually and freely available (SHIPS 2018).

3. Methods, exploration, and findings

The purpose of this paper is to quantify diurnal oscillations of Tb fields discerned from IR data within 600 km of TC centers, to explore environmental factors that may modulate the intensity and/or regularity of these diurnal oscillations, and to determine if there are a set of storm characteristics and environmental conditions that are more favorable for diurnal oscillations in TCs.

a. Quantifying diurnal oscillations with IR data

The CIRA IR archive and the best track data are used to create storm-centered IR imagery on a polar grid that is rotated with respect to storm translation (to the top of the page) using the method described in Knaff et al. (2014). The polar grid has a 4-km radial $\times$ 10° azimuthal grid spacing and extends to a radius of 602 km. A principal component analysis (PCA) is performed on the covariance matrix of IR Tb polar analyses for the entire TC archive. This type of PCA is used to identify or isolate spatial patterns associated with the largest variations in the data (Wilks 2006). The normalized spatial loading factors, or empirical orthogonal functions (EOFs), associated with the first four principal components (PCs) for all cases in the TC IR image archive are shown in Fig. 1. Table 1 provides the variance explained and interpretation of each of these PCs. These spatial patterns are orthogonal (mutually uncorrelated) in space, the coefficients of different EOFs are orthogonal in time, and there is no set of fewer functions (EOFs) that will specify the variance patterns (here, Tb anomalies) as precisely (Barry and Perry 1973). An identical analysis of IR imagery and description of the patterns

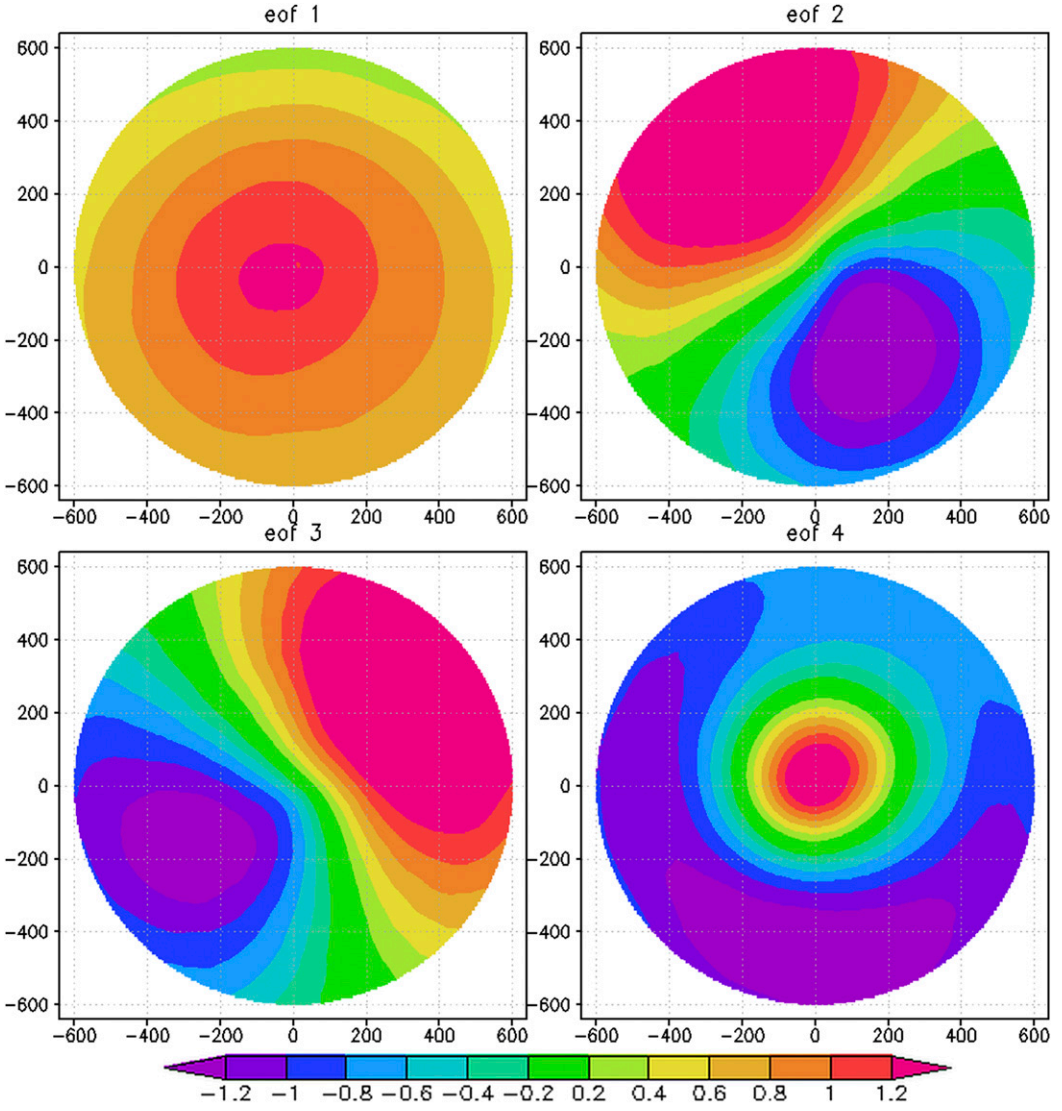

FIG. 1. Normalized patterns associated with the first four principal components of storm direction relative, TC-centered IR images. Descriptions of the spatial patterns are in Table 1 and a detailed discussion can be found in Knaff et al. (2015).

associated with the first 12 EOFs are found in Knaff et al. (2015).

Examining the PCs associated with the fourth empirical orthogonal function (EOF4),[2] which explains 8.9% of the Tb variance, reveals an interesting regular pulsing behavior that seems related to oscillations of cloud-top Tbs that spatially behaves similarly to the diurnal oscillations of the areal extent of TC cirrus canopy in Browner et al. (1977), Muramatsu (1983), Lajoie and Butterworth (1984), and Kossin (2002), and the timing of outward propagation of cloud-top temperatures discussed in D14. We examined the behaviors of PC4 [i.e., variations associated with EOF4 (Fig. 1)], with respect to LST instead of coordinated universal time (UTC) for the cases discussed in D14, and it appears that PC4 is capturing the diurnal variations documented in previous work. Figure 2 shows the normalized PC4 for three of the cases used in D14—PC4 reaches a minimum earlier in the day and a maximum later in the day. This Tb pattern, unlike those in D14 who examines Tb trends/changes occurring over a 6-h period, does not appear to propagate outward, but rather pivots at a radius of

[2] This 2D pattern has a 1D (azimuthally average) counterpart that is used in Knaff et al. (2014, their Fig. 1) to study/estimate TC size variability; suggesting that variations of EOF4 may also be related to TC size variations.

TABLE 1. Interpretation and percent variance explained associated with the EOFs shown in Fig. 1. A more thorough analysis and discussion of the EOFs can be found in Knaff et al. (2015).

IR EOF/PC	Interpretation	Percent variance explained
1	Size/intensity of the cloud shield	32.2
2	Azimuthal wave 1	11.5
3	Azimuthal wave 1, quadrature phase	10.7
4	Symmetric pulsing variability	8.9

approximately 220 km. It is also noteworthy that none of the other PCs examined (1–3) here have similar diurnally oscillating behaviors—this result is consistent with the mutually uncorrelated nature of PCs.

Based on these findings, the hourly averages of PC4 with respect to LST are calculated for all TCs with at least tropical storm (ALL), hurricane (H), and major hurricane (MH) or greater intensities in our dataset. For all three categories of intensity, Fig. 3 shows a vibrant mean diurnal oscillation with a minimum of PC4 in the morning hours, 0300 to 0900 LST, and a maximum in the afternoon hours, 1400 to 1800 LST. The mean amplitude is about 0.3 or 0.4 standardized deviations of the normalized value of PC4, for ALL, H, and MH cases. Because the mean behavior captures the oscillating diurnal pattern, we perform a linear regression between the PC4 observations and the mean variations, shown in Fig. 3, to determine if the TC cases have PC4s oscillating in a similar manner. Since the times of the observations are variable, we use cubic-spline interpolation to provide the value of the mean oscillation at the observation's LST. We use the hourly mean diurnal cycle associated with the ALL sample, given the similarities in shapes of the mean oscillations. The coefficient of determination provides a measure of the goodness of fit (i.e., R^2) and the slope (b) of the regression line provides information about the sign and amplitude of the relationship. Using these two pieces of information, we divide our sample into five categories: strong diurnal (SD), moderate diurnal (MD), neutral (N), moderate antidiurnal (i.e., out-of-phase/negative slope) (MA), and strong antidiurnal (SA), as described in Table 2. The sign of the slope determines if the case is diurnal (+) or antidiurnal (−). For strong and moderate categories, we require that at least 50% or 25% of the variance of an individual 24-h period be explained and the absolute value of the slope b (i.e., amplitude) be greater than 2 and 1, respectively. For each 24-h sample (or case), we require that at least 10 data points (i.e., images) are available to create the regression. Using these categories, the oscillating behavior

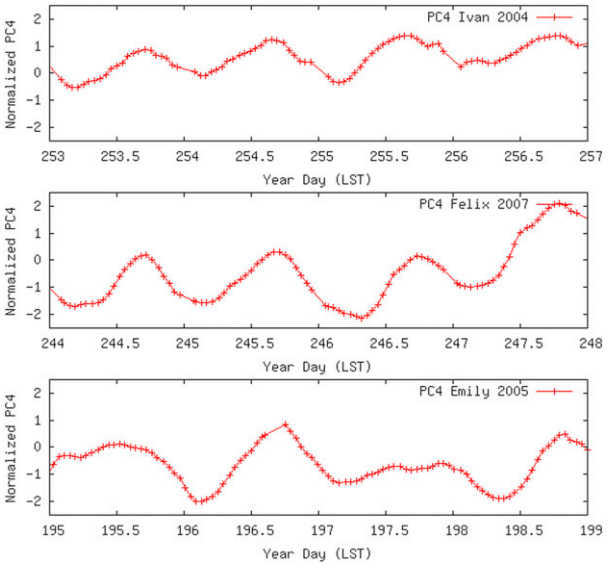

FIG. 2. The 4-day time series of the fourth principal component (PC4) for Hurricanes Ivan (2004), Felix (2007), and Emily (2005), starting on 9 Sep, 1 Sep, and 14 Jul, respectively.

(diurnal cases strong and moderate) occurs in over 45%, 54%, and 61% of the ALL, H, and MH cases, respectively.

As a visual example, Fig. 4 shows the time evolution of the Tb field associated with PC4 with mean amplitudes corresponding to a slope of two and a mean daily value of PC4 equal to zero, which mimics the minimum amplitude of SD cases. In this example, a negative (cold) anomaly (−2°C) develops in the inner-core region and a positive (warm) anomaly (2°C) develops outside 220 km of the TC by 0030 LST and by 0830 LST the inner-core cold anomaly increases in amplitude to less than −5°C and the warm anomaly increase to 4°C outside 220 km. The inner-core negative anomaly erodes and a positive (warm) anomaly greater than 3°C develops by 1630 LST and the warm anomaly beyond 220-km radius erodes and a negative anomaly colder than −3°C develops by 1630 LST. The timing of Tb evolution outside 220 km shows cooling beginning after sunrise (0800 LST) and warming beginning near sunset (1800 LST). Given the thresholds for the five categories, the TCs in the strong diurnal, SD, or strong antidiurnal, SA, categories have Tbs that oscillate over at least a 7°C range from maximum to minimum. It is however difficult from this analysis to determine cloud type (e.g., convective, stratiform, cirrus) or IR optical thickness because the IR data only provides cloud-top Tb information. Based on our classification thresholds, this value is about half the magnitude of the oscillations seen in 6-hourly IR image differences observed in the 31 major hurricanes documented in D14. We expect these amplitude differences due to our

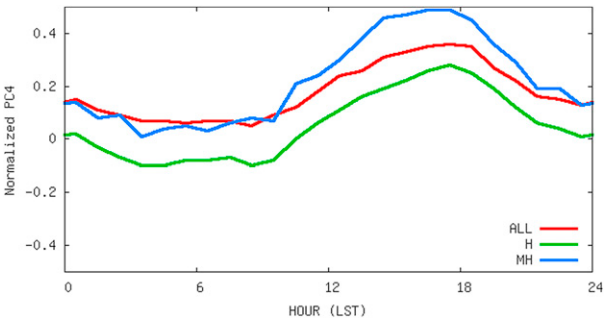

FIG. 3. Mean daily cycle of the fourth principal component (PC4) for all TCs with intensities greater than 34 kt (ALL), hurricane cases or greater than 64 kt (H), and major hurricanes or intensities greater than 95 kt (MH).

classification criteria and the use of a larger more comprehensive dataset in our analysis.

Another way to depict the information shown in Fig. 4 is to show the temporal evolution of the azimuthal mean result. The left panel of Fig. 5 shows the hourly evolution of azimuthally averaged EOF4 corresponding to the ALL PC4 with an amplitude (slope) of two as shaded contours and the spatial and temporal derivative as contours, which again mimics the minimum amplitude of SD cases. The ranges of the D14 clock are shown as red dashed lines. Again, the Tbs are not propagating with a node near 220-km radius. There is also an indication that the cooling inside 220 km is nearly simultaneous with the warming outside 220 km. The time–space derivative show some evidence of slight radial propagation within the diurnal clock ranges outside of 220 km. In fact, when the contour interval is reduced to 0.1 the minimum is seen moving outward between ~240 km at 0900 LST to ~500 km at 1800 LST (not shown). In the right panel of Fig. 5, we try to replicate the 6-hourly differences discussed in D14 by performing a 6-h difference of the Tbs shown in the left panel (shaded) and the temporal and spatial derivatives (contours)—differencing is commonly used to stabilize means and remove trends and seasonality in a time series (Hyndman and Athanasopoulos 2013). In this work, the shaded Tb differences show a slight tendency to propagate outward with time, particularly in 240–500-km radii at approximately 0800–1800 LST. These differences also shift the patterns in time, moving the maximum warming at 400–500 km to just before midnight, where the maximum Tb anomaly occurs at ~0600 LST in the Tbs. The differencing also reduces the magnitude of the oscillations within 220-km radius and shifts the minimums from early to midmorning (left) to just before midnight (right).

There are notable differences between the PCA-based pattern of Tbs and how they oscillate diurnally and the oscillations shown in D14. The temporal evolution of this pattern shown in Fig. 4 does not indicate radial propagation, rather a nearly symmetric diurnal signal where infrared brightness temperatures oscillate from warm to cold and cold to warm within and outside of a radius of approximately 220 km, with maximum central cooling occurring in the early morning (0300–0800 LST), and a nearly simultaneous maximum warming occurring near the 500-km radius. The D14 work also does not find much diurnal variability inside 200 km. The analysis in Fig. 5 shows derivatives moving outward beyond 240 km as well as some of potentially important (for interpretation) differences due to examining 6-h Tb differences instead of Tb anomalies. Thus, we feel the patterns documented here are likely related to the oscillations discussed in D14. But, we ask the readers to recognize that the oscillation is based on variance structures in Tb anomalies—not temporal Tb differences—and that the discrepancies between the two types of analyses are to be expected.

TABLE 2. Slope b and variance explained (R^2) values associated with the five categories of diurnal oscillations used in this study.

Category	Slope b	Variance explained (R^2)
Strong diurnal (SD)	$b \geq 2.0$	$R^2 \geq 0.50$
Moderate diurnal (MD)	$2.0 > b \geq 1.0$	$0.50 > R^2 \geq 0.25$
Neutral (N)	$1.0 > b > -1.0$	$R^2 < 0.25$
Moderate antidiurnal (MA)	$-2.0 < b \leq -1.0$	$0.50 > R^2 \geq 0.25$
Strong antidiurnal (SA)	$b \leq -2.0$	$R^2 \geq 0.50$

b. *Quantifying the TC environment*

With the stratification of TC cases into the SD, MD, N, MA, and SA classifications, we examine the TC large-scale environmental factors associated with each diurnal classification to elucidate environmental differences that may correspond with observed diurnal oscillations of IR Tbs. For this work, we select and investigate basic TC characteristics and environmental factors known to affect TC intensity and structure by using the SHIPS Developmental Dataset (Table 3). The TC characteristics include latitude (LAT), storm speed (SPD), intensity (VMAX), and an IR-based TC size (TCSZ; Knaff et al. 2014). These general characteristics allow us to say if the sample is different (e.g., poleward, faster, weaker, bigger). The environmental factors include deep vertical wind shear (SHDC), generalized vertical wind shear (GSHR), environmental pressure (ENVP), oceanic heat content (OHC), relative humidity in three layers (RHLO, RHMD, RHHI), 200-hPa divergence (D200), 200-hPa relative eddy flux convergence (REFC), the 850- to 700-hPa temperature advection (TADV), the 500-km tangential winds at 850 hPa (VT85) and 300 hPa

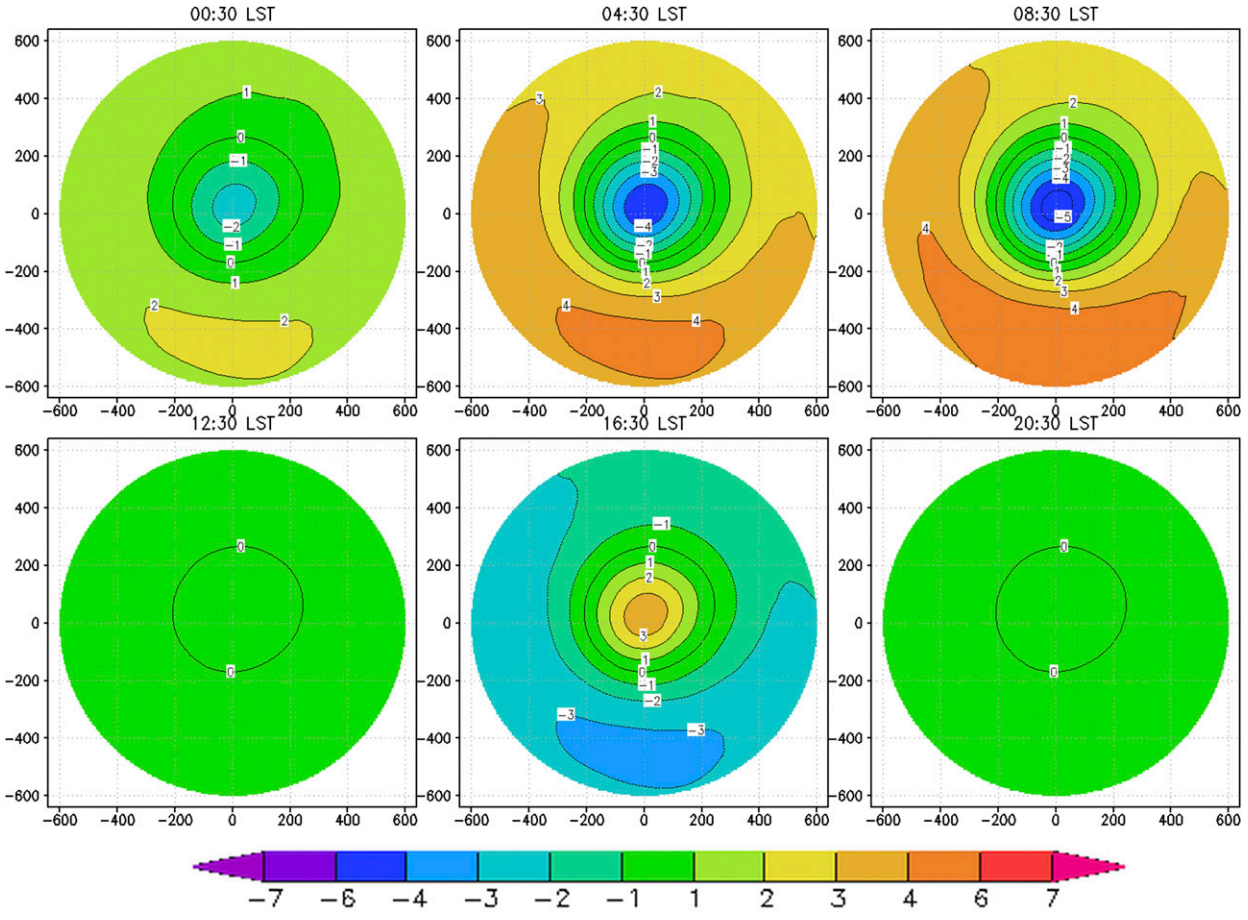

FIG. 4. Example of the IR Tb changes associated with the fourth principal component (PC4) amplitudes that are twice as large as the observed mean diurnal oscillation associated with all TC cases with intensities greater than 34 kt in the best track files. These idealized depictions mimic the behavior observed with strongly diurnal (SD) cases as defined in this study.

(VT30), and the temperature at 150 hPa (T150), 200 hPa (T200), and 250 hPa (T250). Using the SHIPS Developmental Dataset, average environmental conditions are calculated over the daylong period when the diurnal oscillations are quantified/observed. To aid the reader and limit verbosity, Table 3 provides information on how the parameters are calculated, units, and a description of what each environmental factor represents.

For these TC characteristics and environmental conditions, relatively simple Student's *t*-test statistics [Student (William S. Gosset) 1908] are calculated to conduct hypothesis testing to determine if differences in mean values are statistically different assuming independent samples while recognizing that the samples will be reduced by the time between independent samples (Leith 1973; Wilks 2006). To be very conservative, we will assume that time is 24 h, which reduces the degrees of freedom by a factor of 2.7. We also increase the intensity stratifications by adding minor hurricanes (mH) and tropical storms (TS), with intensities ranging from 64 to 96 kt (where 1 kt = 0.5144 m s^{-1}) and 34 to 64 kt, respectively. These composite differences tell us what factors have significant mean differences. We will use these categories for intensity. However, we keep the discussion of composite and regression results (in section 3c) to ALL, TS, mH, and MH categories for brevity.

With the majority of TCs showing some amount of diurnal oscillations, we first examine the mean spatial variability of the regression coefficient for our combined sample (ALL) as shown in Fig. 6. Note that overland cases are used here to examine if proximity to land can be used to infer obvious changes in diurnal behavior. A two-pass Barnes (1964) analysis is used to map the regression coefficient to an even latitude by longitude grid from the combined ALL sample (i.e., an estimate of the spatial mean value at that latitude and longitude point). For the first and second pass, the radius of influence is 1500 and 500 km and the *e*-folding distance is 750 and 500 km, respectively. This analysis allows us to see where the diurnal oscillations, in a spatial mean sense, are most

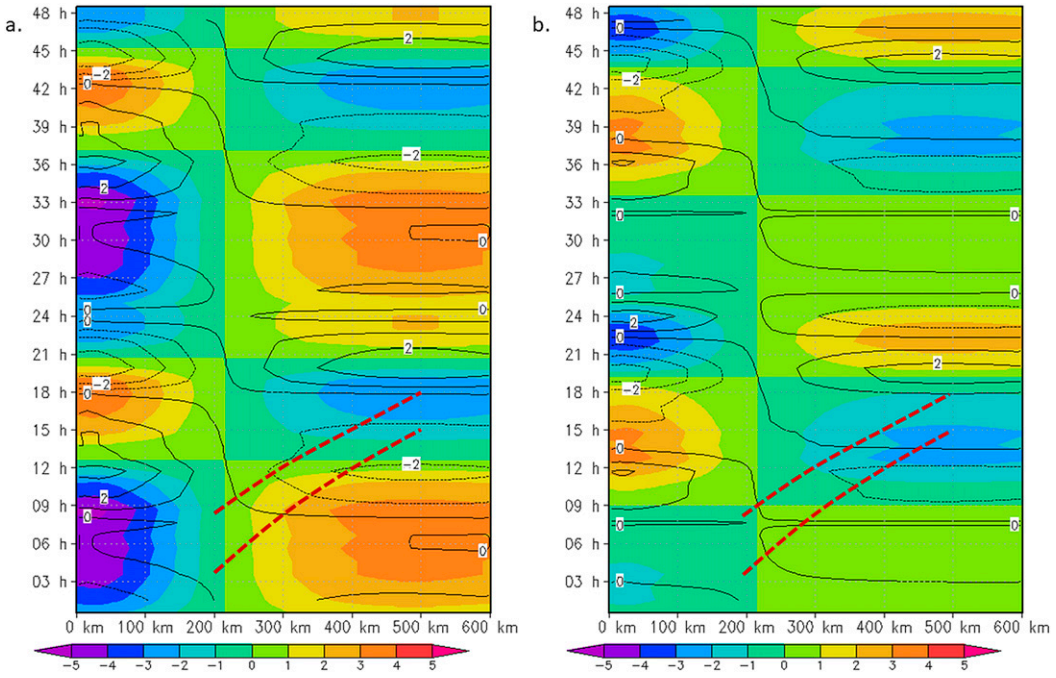

FIG. 5. Two diurnal cycles with respect to LST of the radius vs time depiction of the azimuthally averaged behavior of (a) EOF 4 and (b) EOF 4 minus the values of EOF 4 from 6 h earlier. Both plots show the temperature variations associated PC values that are twice the observed mean diurnal oscillation associated with all TC cases with intensities greater than 34 kt (i.e., ALL) (shaded), the derivative temperature variations with respect to time and radius (black contours), and the ranges of the diurnal clock presented in D14 are indicated by the red dashed lines. These idealized depictions mimic the behavior observed with strongly diurnal (SD) cases as defined in this study.

in and out of phase with the mean diurnal oscillation that is shown in Fig. 3. Keeping the number of cases used in the analysis (Fig. 6, top) in mind, Fig. 6 (middle) shows that the largest in-diurnal-phase response is mostly confined to the latitudes equatorward of 25° and generally where the most intense storms occur, Fig. 6 (bottom). Proximity to land also does not noticeably appear to influence diurnal behaviors of TCs. Of note, the strongest diurnal oscillations (positive R) occur in the Gulf of Mexico, far eastern and central equatorial Pacific, and in the Indian Ocean (Fig. 6, middle). Strong antidiurnal-phase responses (negative R) are found in areas with strong subtropical high pressure centers and SSTs cooler than 26°C. These regions are typically located in the central North Pacific and eastern North Atlantic. While this suggests that the environment may be playing a role in the strength and phase of the TC diurnal oscillation, the results offer no clear indication of the environment factors or storm characteristics that modulate the diurnal oscillations. For instance, the subtropical high regions typically have lower underlying sea surface temperatures, exhibit upper-level convergence, contain drier conditions in the mid- and upper levels, possess higher SHDC and GSHR, and thus support the development of weaker TCs.

Using the same cases as Fig. 6, we perform a composite analysis to further examine the environmental factors and storm characteristics (see Table 3) for TS, mH, and MH cases. Table 4 shows the composite means of our five diurnal stratifications for each of these intensity classes. In this table, only the mean conditions for the SD cases and those means that are significantly different (using a Student's t test with reduced degrees of freedom) from the SD composite means are shown. Of note, the TS and mH cases have quite similar composite results. The SD cases appear to occur at equatorward LAT, slower SPD, and higher VMAX. TCSZ did not significantly vary with the diurnal cycle—this is true for all diurnal oscillation categories and is not discussed. All SD cases are associated with environments that have lower SHDC and GSHR, higher OHC, higher values of RHHI[3] and RHMD,[4] lower TADV, and colder T150 conditions. Examining just MH cases, SD cases occur at poleward LAT, faster SPD, lower D200, and more TADV than the other diurnal stratifications. The latter finding may suggest that environmental conditions

[3] Sample mean values of RHHI are 58%–59%.
[4] Sample mean values of RHMD are 62%–63%.

TABLE 3. A list of storm characteristics from the TC best track database files and environmental factors derived from the SHIPS Developmental Dataset used in this study along with a brief description and acronyms that will be used in the text.

Acronym	Units	Description
		Storm characteristics
LAT	° latitude	Latitude of the TC center
SPD	kt	Storm motion speed
VMAX	kt	Maximum intensity of the storm
TCSZ	° latitude	IR-based TC size parameter (Knaff et al. 2014)
		Environmental predictors (time averaged from $t = 0$ to $t = 24$ h)
SHDC	kt	850–200-hPa wind shear magnitude within 500 km of the TC
GSHR	kt	850–200-hPa generalized wind shear calculated as the mass-weighted root-mean-square deviations of the winds from the mass-weighted deep-layer mean winds times a factor of 4 calculated in a 200–800-km annulus (Knaff et al. 2005)
ENVP	hPa	200–800-km average surface pressure
OHC	kJ cm^{-2}	Oceanic heat content between the surface and the depth of the 26°C isotherm (Shay et al. 2000, and references within)
RHLO	%	850–700-hPa relative humidity averaged within a 200–800-km annulus
RHMD	%	700–500-hPa relative humidity averaged within a 200–800-km annulus
RHHI	%	500–300-hPa relative humidity averaged within a 200–800-km annulus
D200	$\times 10^{-7}$ s^{-1}	200-hPa divergence calculated in a 1000-km circle
REFC	m s^{-1} day^{-1}	Average relative eddy momentum flux convergence calculated in 100–600-km annulus vs time (DeMaria et al. 1993)
TADV	$\times 10^{-6}$ °C s^{-1}	Temperature advection between 850 and 700 hPa averaged from 0 to 500 km, and calculated from the geostrophic thermal wind
VT85	$\times 10^{-1}$ m s^{-1}	850-hPa tangential wind azimuthally averaged at $r = 500$ km from the TC center
VT30	$\times 10^{-1}$ m s^{-1}	300-hPa tangential wind azimuthally averaged at $r = 500$ km from the TC center
T150	°C	200–800-km area average 150-hPa temperature
T200	°C	200–800-km area average 200-hPa temperature
T250	°C	200–800-km area average 250-hPa temperature

associated with MHs are generally most favorable for diurnal oscillations, echoing the conclusions of Muramatsu (1983) and D14. In our 2005 to 2015 sample, 61% of major hurricanes show in-phase diurnal oscillations (e.g., SD and MD). In accessing all five of the diurnal stratifications for MH cases, we note that conditions are favorable for TC intensity increase in that SHDC is less than 10 kt, GSHR is less than 22 kt, OHC > 60 kJ cm^{-2}, RHMD is greater than 64%, RHHI is greater than 59%, D200 is greater than 1×10^{-7} s^{-1}, and TADV is in a range of 0° to 3×10^{-6} °C s^{-1}. We think this result indicates that environmental and storm characteristic conditions associated with MHs are generally favorable for diurnal oscillations and causes of out-of-phase behavior is likely due to factors not explicitly examined nor captured in our analysis.

It is also remarkable that a large percentage of weak TC cases exhibit diurnal oscillations. In total, 41% and 51% of TS and mH cases have indications of in-phase diurnal oscillations, respectively. The percentages for TS (41%), mH (51%), and MH (61%) presented here are similar, although a bit lower, to those found by Ditchek et al. (2019), who examined the same 6-hourly IR differences as D14 in the Atlantic basin (1982–2017), developed a different diurnal metric based on D14's clock for classification, and found TS (46.0%), mH (63.8%), and MH (79.5%) have long-lived cold pulses in IR images. The pervasiveness of diurnal variations in all TCs is a fortuitous result in that we can explore the significant differences found in this larger sample of ALL TC cases and look beyond the MH environments that are very similar among the different diurnal stratifications. We will concentrate on the environmental factors SHDC, RHHI, TADV, and T150 to look for the largest differences in the ALL cases composites where the weaker cases dominate.

Figure 7 shows the zonal mean values of VMAX, RHHI, SHDC, TADV, and T150 associated with ALL intensities for each of the diurnal stratifications. This allows for a closer examination of the latitudinal behavior of the environmental conditions that appears to be most related to the strength and regularity of the diurnal convection in TCs. Figure 7a shows that SD and MD cases are generally more intense, again agreeing with D14 and Ditchek et al. (2019). Figure 7b shows the zonal means of RHHI—for most cases (e.g., in latitudes from 15° to 30°), it appears that higher RHHI values are typically related to more pronounced diurnal oscillations. Again, equatorward of 30°, Fig. 7c shows that lower vertical wind shears are associated with more

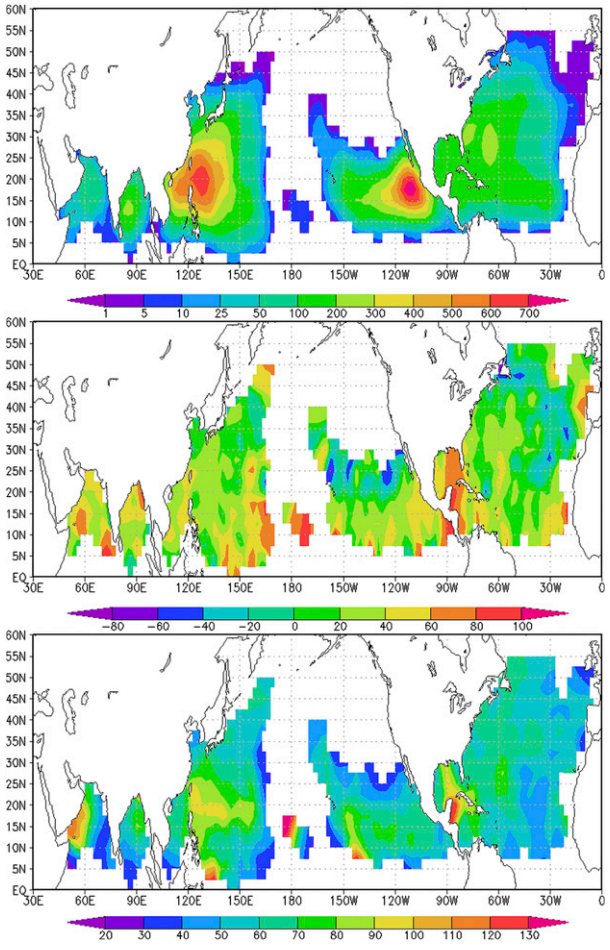

FIG. 6. The figure is created using a two-pass Barnes (1964) analysis with 1500 and 500 km being used as the radius of influence and 750 and 500 km *e*-folding distances being used in the first and second pass, respectively. (top) The number of cases used in the second pass of the Barnes analysis, (middle) regression coefficient/diurnal strength (R) between the mean IR diurnal oscillation in tropical cyclones and observed storms, and (bottom) the mean intensity (VMAX).

pronounced diurnal cycling. Figures 7d and 7e show that TADV and T150 are not as clearly stratified as a function of diurnal oscillation strength, though slightly lower TADV and cooler T150 seem more common for diurnally oscillating TCs equatorward of 30°. These analyses are suggesting that SHDC and RHHI may be more important environmental factors for diurnal oscillations of TCs than TADV or T150. However, as is the case with the composite analyses, it remains difficult to untangle the environment from the intensity. In an additional attempt to separate the environmental and intensity factors, section 3c presents regression-based results.

c. *Regression analysis of the environment*

The environmental and tropical cyclone data associated with the diurnal cases is rather noisy and the environmental factors are covarying. Here we examine multiple linear regressions to help determine which factors are, relative to each other, more important in the observed diurnal variability and where the diurnal variability is most sensitive to those factors. We use a simple averaging strategy to reduce the variability and regression analysis to address the issue of colinearity. To create an averaged dataset that covers the variability found in the original data, we sort the cases by regression coefficient between hourly LST average PC4 and observed PC4 (R) or diurnal strength, VMAX, SHDC, RHHI, and TADV—noting that T150 did not have any significant variability with R, but TADV did. Once sorted, we create an averaged dataset using increments of 100 cases. This data chunking procedure results in five averaged data series that are 97 cases long for a total of 485 average scenarios that we then apply multiple regression to; regressing VMAX, SHDC, RHHI, and TADV against R. This ensures that we cover much of the dimensionality of the original dataset. Table 5 shows the result of the multiple regression that explained 15% of the variance in the averaged sample. Regression analysis results provide different deductions. Results suggest that higher values of RHHI and VMAX are important to the diurnal variation of TC cloud-top IR brightness temperatures and that TADV and SHDC likely play a lesser, but potentially important role in modulating the strength and phasing of TC diurnal oscillations.

The multiple regression analysis also lets us examine the residuals in the multiple regression as a function of each individual variable; effectively removing the contributions of the other independent variables. Figure 8 shows the residuals associated with VMAX, SHDC, RHHI, and TADV—the interpretation of the residuals needs some explanation. Residuals are predicted minus observed and as a result the signs of the residuals are opposite of the sign of the relationship. Additionally, residuals are calculated holding the variability of other independent variables fixed, which removes collinearity amongst the independent variables. Slight positive (i.e., VMAX, RHHI) and negative (i.e., SHRD, TADV) residual slopes indicate systematic negative and positive errors in the regression relationships (or under forecasting), which is typical of squared error minimization approaches. Finally, larger scatter in the residuals indicates that the fit is less certain. We concentrate on ranges of each environmental factor where the relationship with diurnal TC oscillations is poorest, which is another way at looking at the sensitivity of these factors to diurnal oscillations of TC convection.

TABLE 4. Composite analyses of tropical cyclones stratified by their diurnal classification and intensity. Bold, italic, and plain fonts represent statistical significance at the 99%, 97.5%, and 95% relative to the strong diurnal cases. Only variables with statistically significant differences are shown.

Variable	Strong diurnal	Moderate diurnal	Neutral	Moderate antidiurnal	Strong antidiurnal
			Tropical storms (TS)		
No. (%) of cases	1045 (14%)	1977 (27%)	3115 (43%)	844 (12%)	328 (4%)
LAT	18.95	*19.63*	**21.05**	**22.73**	**22.77**
SPD	9.82		10.21	*10.47*	
SHDC	13.32	13.78	**14.89**	**15.52**	**14.86**
GSHR	23.75		**25.37**	**26.43**	**25.62**
OHC	45.84	*42.01*	**38.08**	**31.47**	**27.53**
RHMD	65.44	*64.44*	**62.93**	**60.28**	**61.00**
RHHI	59.61	*58.29*	**56.35**	**52.54**	**52.87**
D200	0.30		*0.12*		
TADV	1.30		*2.00*	**2.94**	**2.47**
T150	−66.67		−66.27	**-65.94**	**-65.79**
			Minor hurricanes (mH)		
No. (%) of cases	635 (17%)	1275 (34%)	1480 (40%)	263 (7%)	70 (2%)
LAT	20.22		**21.81**	**22.76**	**24.60**
SPD	10.28			**11.25**	**12.24**
VMAX	78.27		**76.30**	**75.00**	**72.84**
SHDC	11.95		12.55	**13.89**	**13.92**
GSHR	22.53		**23.61**	**25.99**	**25.77**
OHC	43.48			**38.22**	**35.00**
RHMD	65.18	64.06	**62.56**	**59.69**	**58.24**
RHHI	59.50	58.22	**56.27**	**53.38**	**52.50**
TADV	1.61		**3.29**	**4.94**	**5.60**
T150	−66.39	−66.22	**-65.99**	**-65.73**	**-65.37**
			Major hurricanes (MH)		
No. (%) of cases	442 (21%)	842 (40%)	689 (33%)	105 (5%)	35 (2%)
LAT	19.18			**18.00**	**17.41**
SPD	10.53		**9.79**	**8.63**	**6.89**
OHC	61.30		64.96	**68.23**	**69.73**
D200	0.76			**2.75**	**7.00**
TADV	2.09				**0.55**

The multiple regression residuals as a function of VMAX show that the largest residual scatter is confined below ~75 to 80 kt—an intensity that is associated with the first persistent eye in IR imagery (Vigh et al. 2012). The residual analysis as a function of SHDC, which is the weakest factor in the multiple regression, shows that diurnal oscillations are most sensitive in the range of 10 to 17 kt. These SHDC ranges are higher than values that are typically favorable for intensification (DeMaria and Kaplan 1999; DeMaria et al. 2005; Kaplan et al. 2010; Knaff et al. 2005, 2018) and have been often referred to as moderate shear in the literature. The residuals associated with RHHI suggest that the greatest diurnal oscillation sensitivity in TCs occurs when the RHHI values are between ~50%–64%. Higher values of RHHI seem related to more pronounced TC diurnal oscillations and those oscillations are likely under predicted by the regressions developed here. RHHI values below 50% are generally negatively related to R and have small residuals. This may explain the propensity of diurnal oscillations associated with storms in the Gulf of Mexico, western Caribbean, and Bay of Bengal (see Fig. 6) as these are regions with climatologically higher mid- and upper-level humidity values. Similarly, diurnal oscillation sensitivity from temperature advection is found in a narrow band between roughly 0 and 5×10^{-6} °C s^{-1} suggesting that large values of temperature advection inhibit the diurnal oscillations of convection. This is likely important for those storms interacting with the midlatitudes or transitioning to extratropical cyclones.

d. *Application to storms in the 2018 tropical cyclone season*

In this section, we apply our findings based on data from 2005 to 2015 to an examination of the diurnal oscillation categories and mid- and upper-level relative humidity values in tropical cyclones during the 2018 North Pacific tropical cyclone season. Figure 9 shows the evolution of major Hurricane Hector (left panels) and Typhoon Maria (right panels)—note that the data is

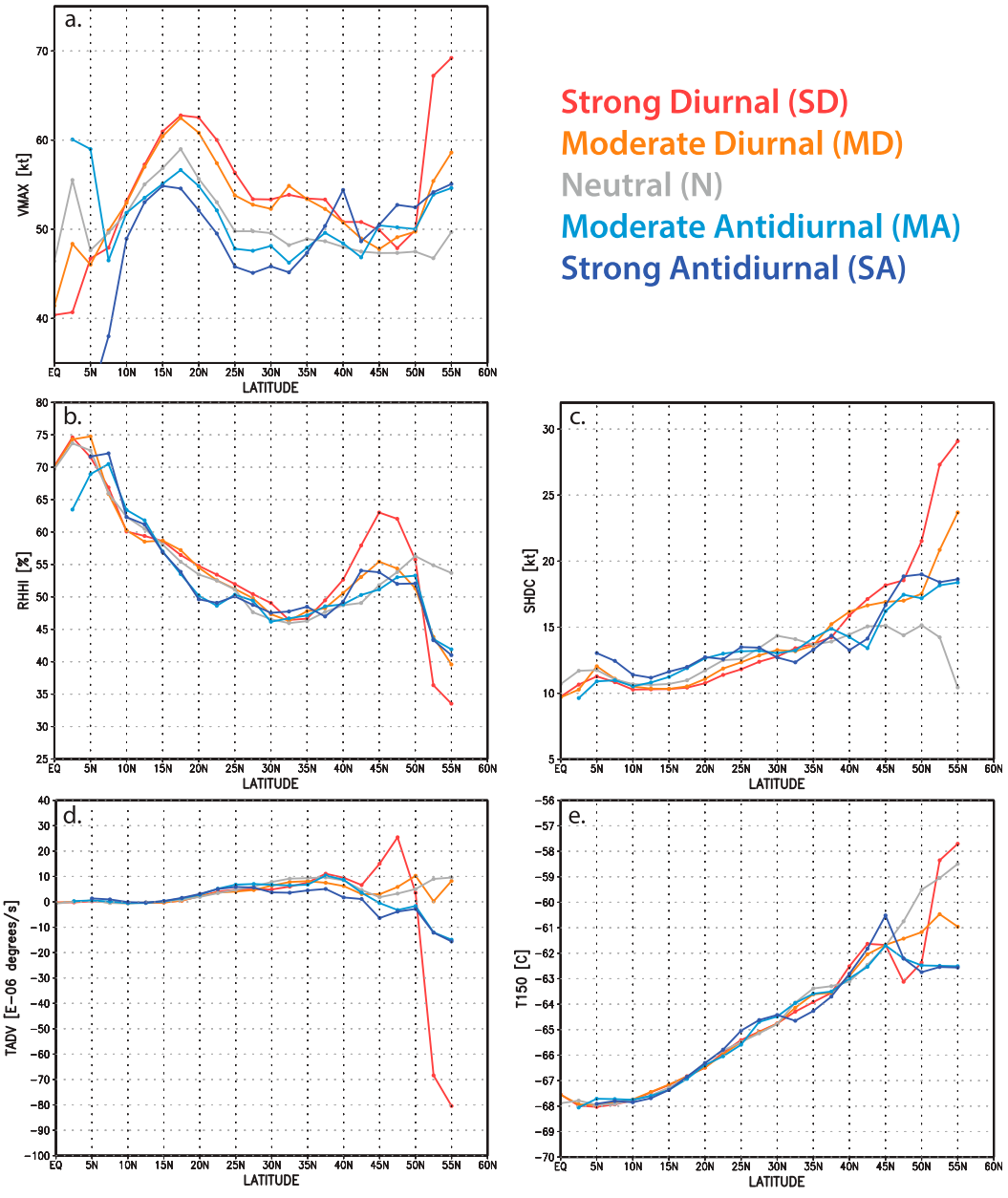

FIG. 7. Zonal mean values of (a) VMAX, (b) RHHI, (c) SHDC, (d) TADV, and (e) T150 environmental factors associated with all tropical storm and hurricane cases (ALL) and stratified by diurnal classification. Strong diurnal, moderate diurnal, neutral, moderate antidiurnal, and strong antidiurnal stratifications are shown in red, orange, gray, light blue, and blue, respectively.

based on the 2018 operational SHIPS dataset (i.e., values are calculated from 6-h forecasts) and preliminary best track files. Both systems underwent genesis with a moderate amount of environmental moisture—this elevated moisture content corresponds with moderate to strong diurnal oscillations. Both systems also reached major hurricane/typhoon intensities (>96 kt) and maintained those intensities for many days—indicating that the environment with respect to ocean and atmospheric conditions remained rather favorable for intensification and maintenance. However, as the systems mature and reach their peak intensity, the favorability of environmental moisture deviates between the two systems that manifests itself in the diurnal oscillation. As hurricane Hector tracks from the eastern to the central North Pacific and the environment around the storm dries as evidenced by the mid- and upper-level relative humidity, Hector exhibits a neutral diurnal

TABLE 5. Results of the averaged variable multiple regression analysis vs *R*. The multiple linear regression explained 15% of the variance in this averaged sample. Student's *t* test probabilities based on a one-tailed test as the signs of the relationships are known based on prior composite analysis.

Variable	Coefficient	*t* statistic	*P* value
Intercept	−62.6322	−3.621 74	0.000 318
VMAX (kt^{-1})	0.568 652	4.506 956	7.97×10^{-6}
SHDC (kt^{-1})	−0.79 134	−1.5691	0.117 172
RHHI ($\%^{-1}$)	1.125 289	5.243 254	2.22×10^{-7}
TADV [$(10^{-6} \times °C\,s^{-1})^{-1}$]	−0.83 161	−1.854 54	0.064 173

oscillation as shown by the top-left panel in Fig. 9—the value of the slope of the regression line (*b*) for the periods classified as moderate diurnal are between 1.0 and 1.4. The environment around Typhoon Maria stays moist while the intensity of the system is in a quasi-steady state period. Maria retains a robust diurnal oscillation—the value of *b* is between 1.7 and 2.0 during periods classified as moderate diurnal (cf. Table 2). As the storms change intensities and begin to experience environmental changes, the jumps between the diurnal oscillation classifications shown in the top row of panels in Fig. 9 are consistent with the sensitivities highlighted by the regression analysis of the environment in section 3c and Fig. 8. While we only highlight two cases here, both Hector and Maria suggest that our classifications and interpretation of the of typical environmental conditions for diurnal oscillations are relatively robust and are likely indicative of a larger pattern that might be responsible for the discrepancies we see in the diurnal cycle literature (e.g., Kossin 2002; D14). We also examined a couple other relatively long-lived TCs and found similar behavior (not shown). Hurricane Lane (2018) exhibited pronounced diurnal oscillations when the storm had intensities above 80 kt and relatively high values of mid- and upper-level relative humidity. Hurricane Florence (2018), which had a more complicated evolution, displayed less diurnal regularity, but nonetheless a similar behavior.

4. Synthesis, discussion, and hypothesized implications of findings

Knaff et al. (2015) note that in TC IR imagery the fourth EOF/PC exhibits a symmetric pulsing variability pattern. In section 3, we extend this interpretation by linking PC4 to the diurnal variability observed in the IR data. PC4 is one of several IR-based metrics that can be used to capture the diurnal oscillation (e.g., Kossin 2002; D14). However, the benefit of PC analysis is that it represents a robust statistical approach whose spatial patterns and temporal evolutions are mutually uncorrelated and represent the most efficient representation of the variance in a dataset (see Barry and Perry 1973; Bretherton et al. 1992; Wilks 2006). The PC analysis has allowed us to partition the degree of the diurnal oscillation variability (e.g., diurnal, neutral, antidiurnal) in Northern Hemisphere TCs without forcing the

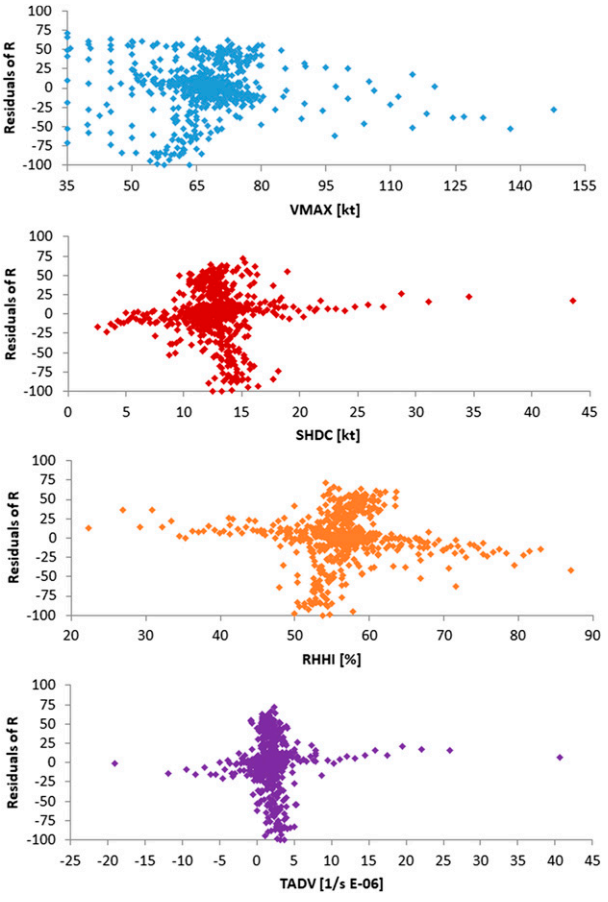

FIG. 8. Residual analysis from the multiple regression analysis of environmental factors related to the diurnal oscillation of IR convection in tropical cyclones. These factors are intensity (VMAX; blue), vertical wind shear (SHDC; red), 500–300-hPa relative humidity (RHHI; orange), and the temperature advection in the 850- to 700-hPa layer (TADV; purple). Residuals are presented as a function of these individual factors with the other environmental factors held constant.

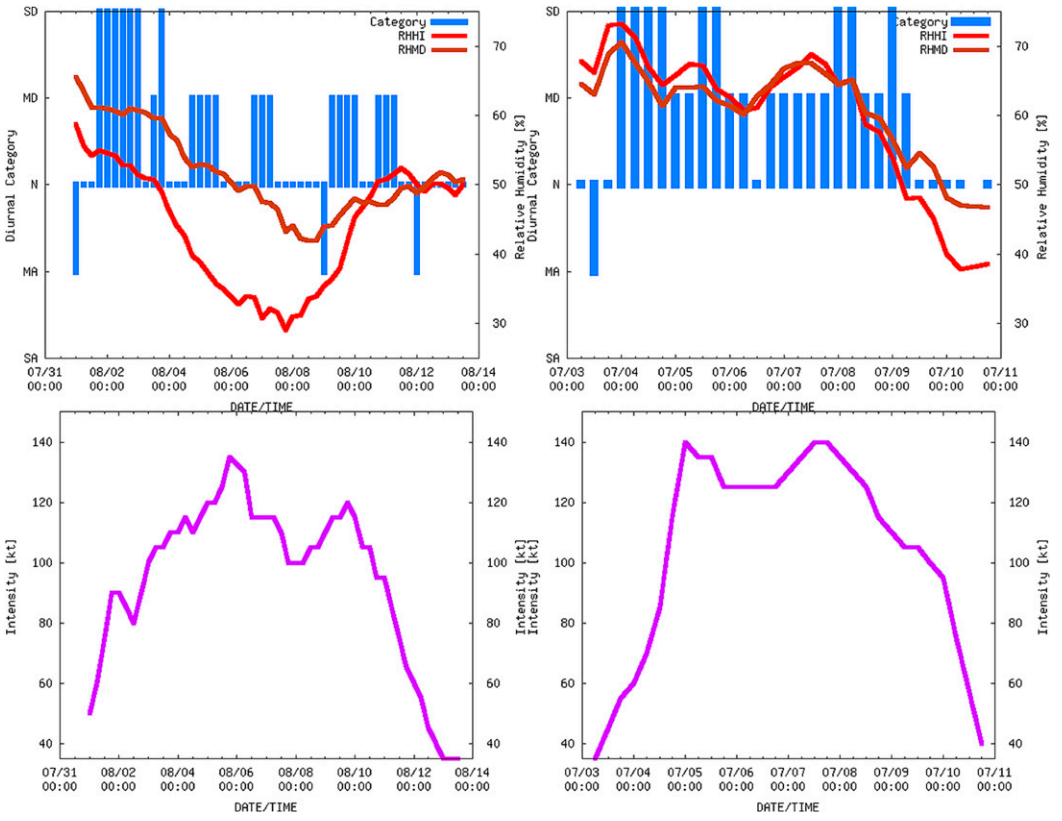

FIG. 9. (top) IR-based diurnal oscillation stratifications (blue bars), RHMD (brown lines), and RHHI (red lines) and (bottom) 1-min sustained wind estimates for (left) Hurricane Hector (2018, ep102018) and (right) Typhoon Maria (2018, wp102018). The values of RHMD and RHHI are based on the operationally produced SHIPS diagnostics and intensities shown and positions used for IR image centering are based on preliminary/working best track files. Date and time are in UTC.

specification of a radial region, differencing period, or brightness temperature threshold. Given our different approach, it is rather encouraging to see other recent work (see Ditchek et al. 2019) also endorse categorizing the type of diurnal signal present in observed TCs.

The data analysis presented in section 3 provides a picture of what storm characteristics and storm environments are associated with distinct and regular diurnal oscillations of deep convection in TCs. Such storms generally move at close to 10 kt forward speed and are located at slightly equatorward latitudes. More intense storms, especially those with hurricane/typhoon strength, are also associated with diurnal oscillations of convection. The favored environment is one with lower vertical wind shear with values that are favorable for intensification ($<\sim$15 kt, 8 m s^{-1}) (DeMaria and Kaplan 1994, 1999; DeMaria et al. 2005; Knaff et al. 2005, 2018; Velden and Sears 2014). Thermodynamically, diurnally oscillating TCs are generally located over higher heat content water ($>$30 kJ cm^{-1}), have cooler temperatures aloft, and higher relative humidity in the mid- and upper levels ($>$62% and $>$58% in the 700–500- and 500–300-hPa layers, respectively). While not the focus of their work, Ditchek et al. (2019) note similar changes in relative humidity in their North Atlantic sample. Finally, relatively small but positive temperature advection also characterizes the environment.

A total of 45%, 54%, and 61% of at least tropical storm-strength, hurricane-strength, and major hurricane-strength TC cases have moderate or strong diurnal signals. In those cases, the general storm and environmental conditions supporting diurnally oscillating TCs is one that supports a symmetric vortex (e.g., higher intensity, lower vertical wind shear, average forward motion) with only small amounts of baroclinic interaction (e.g., positive yet small temperature advection). The thermodynamics are supportive of deep convection (e.g., higher heat content, cool aloft, higher relative humidity values surrounding the core). Of these factors, higher intensities and moister upper-level environments are found to be slightly more important than vertical wind shear and temperature advection. The sensitivity analysis furthermore suggests

that 500–300-hPa environmental humidity (RHHI) tends to be greater than 61% in that layer for TCs that oscillate diurnally and TCs that have higher intensities (>80 kt). These observations imply that TCs possessing hurricane/typhoon like structures—TCs that are typically more symmetric and have eyewall structures intact or developing—are likely to oscillate diurnally. However, the mid- and upper-level relative humidity is related to the amplitude and regularity of the diurnal oscillations in deep convection associated with TCs.

Previous work on diurnal variability of the hydrologic cycle (Randall et al. 1991) found that simulated tropical oceanic convection could be forced solely by the day–night solar heating ''direct radiation–convection interactions'' of clouds and mentioned that other processes could also promote a similarly phased diurnal response, namely ''radiation–dynamics–convection interaction'' (Gray and Jacobson 1977) and ''remote influences of continents'' (Silva Dias et al. 1987). Nicholls (2015) and Ruppert and Hohenegger (2018) tend to support the notion that diurnal variations in organized, deep-convective systems are modulated primarily by the mechanism described in Gray and Jacobson (1977). In the TC case, we feel that it is likely that higher relative humidity in the environment would likely lead to less entrainment and deeper convection, all other factors held constant. This is important because we also know that tropical cyclones have broad upward motion associated with their secondary circulation (e.g., Schubert and Hack 1982) and have mean positive vertical motions at 3 km in most regions of the TC, save possibly the stratiform regions (Black et al. 1996). The oscillations in the IR Tbs within the near-core region (within about 220 km) appear nearly simultaneously with the warming beyond 220 km (Fig. 5), and from examining several cases appear to originate just outside the coldest Tb ring, which is associated with the eyewall. Secondary circulations are also stronger in more intense TCs (Pendergrass and Willoughby 2009), and in less vertically sheared TCs (Riemer and Laliberte 2015). We also know that large values of positive low-level temperature advection are related to TCs that are undergoing extratropical transition (Jones et al. 2003) that disrupts and tilts the secondary circulation, resulting in the development of azimuthal asymmetries.

The near-core region of tropical storms is characterized by conditional convective instability and weak upward motion. In this region, both the direct radiation–convective interaction and the large-scale radiative cooling mechanisms promote diurnal cooling and destabilization of the upper and midlayers of the atmosphere. It is hypothesized that in the region surrounding the eyewall, cooling mostly via large-scale radiative cooling mechanisms triggers moist convection, but ambient relative humidity plays a critical role in either promoting deep penetrating convection to develop or in hindering its development in an on or off manner. Simply stated, if ambient mid- and upper-level relative humidity surrounding the eyewall is above a relatively moist critical value, entrainment is weak enough to allow deep convection to be triggered by the documented direct and indirect radiational cooling mechanisms. Thus, in the neutral diurnal cases with drier mid- and upper-level relative humidity, it is likely that the large-scale radiative cooling mechanism cannot cool a dry environment enough to promote a nocturnal pulse in deep convection nor upper-level clouds. This finding may help to explain why some work does not detect strong or moderate diurnal pulses (e.g., Kossin 2002). *In our assessment, since stronger TCs are generally symmetric and occur in favorable thermodynamics with weak temperature gradients and lower wind shear environments, the mid- and upper-level relative humidity is the key factor for promoting robust diurnal oscillations of IR brightness temperatures and rainfall, with their minima and maxima, respectively, occurring in the early morning. The nearly instantaneous response in Tbs outside the core is likely due to corresponding changes in the secondary circulation.* While many modeling studies have focused on the impacts of changing radiation (e.g., Fovell et al. 2016; Melhauser and Zhang 2014) or depth of the tropopause (i.e., O'Neill et al. 2017), environmental moisture variation in the mid- and upper troposphere has not been investigated in the context of tropical cyclone diurnal oscillations. In future work, we hope to explore further our hypothesis using a combination of observations (rainfall and convection) and simple numerical model simulations.

Acknowledgments. The authors wish to thank Dan Lindsey, Jack Dostalek, James Ruppert, and two anonymous reviewers for their thoughtful comments on this manuscript. The first author would like to thank National Oceanic and Atmospheric Administration (NOAA), his employer, for the opportunity to work on this project. Special thanks go to the Geostationary Operational Environmental Satellite Program Office and NOAA's Hurricane Forecast Improvement Program for providing funding under NOAA Grant (NA17RJ1228) at the Cooperative Institute for Research in the Atmosphere at Colorado State University for the second and third authors of this work, respectively. The views, opinions, and findings contained in this report are those of the authors and should not be construed as an official NOAA or U.S. government position, policy, or decision.

REFERENCES

Barnes, S., 1964: A technique for maximizing details in numerical weather map analysis. *J. Appl. Meteor.*, **3**, 396–409, https://doi.org/10.1175/1520-0450(1964)003<0396:ATFMDI>2.0.CO;2.

Barry, R. G., and A. H. Perry, 1973: *Synoptic Climatology, Methods and Applications*. Methuen, 555 pp.

Black, M. L., R. W. Burpee, and F. D. Marks, 1996: Vertical motion characteristics of tropical cyclones determined with airborne Doppler radial velocities. *J. Atmos. Sci.*, **53**, 1887–1909, https://doi.org/10.1175/1520-0469(1996)053<1887:VMCOTC>2.0.CO;2.

Bowman, K. P., and M. D. Fowler, 2015: The diurnal cycle of precipitation in tropical cyclones. *J. Climate*, **28**, 5325–5334, https://doi.org/10.1175/JCLI-D-14-00804.1.

Bretherton, C. S., C. Smith, and J. M. Wallace, 1992: An intercomparison of methods for finding coupled patterns in climate data. *J. Climate*, **5**, 541–560, https://doi.org/10.1175/1520-0442(1992)005<0541:AIOMFF>2.0.CO;2.

Brier, G. W., and J. Simpson, 1969: Tropical cloudiness and rainfall related to pressure and tidal variations. *Quart. J. Roy. Meteor. Soc.*, **95**, 120–147, https://doi.org/10.1002/qj.49709540309.

Browner, S. P., W. L. Woodley, and C. G. Griffith, 1977: Diurnal oscillation of area of cloudiness associated with tropical storms. *Mon. Wea. Rev.*, **105**, 856–864, https://doi.org/10.1175/1520-0493(1977)105<0856:DOOTAO>2.0.CO;2.

Ciesielski, P. E., R. H. Johnson, W. H. Schubert, and J. H. Ruppert, 2018: Diurnal cycle of the ITCZ in DYNAMO. *J. Climate*, **31**, 4543–4562, https://doi.org/10.1175/JCLI-D-17-0670.1.

DeMaria, M., 2009: A simplified dynamical system for tropical cyclone intensity prediction. *Mon. Wea. Rev.*, **137**, 68–82, https://doi.org/10.1175/2008MWR2513.1.

——, and J. Kaplan, 1994: A Statistical Hurricane Intensity Prediction Scheme (SHIPS) for the Atlantic basin. *Wea. Forecasting*, **9**, 209–220, https://doi.org/10.1175/1520-0434(1994)009<0209:ASHIPS>2.0.CO;2.

——, and ——, 1999: An updated Statistical Hurricane Intensity Prediction Scheme (SHIPS) for the Atlantic and eastern North Pacific basins. *Wea. Forecasting*, **14**, 326–337, https://doi.org/10.1175/1520-0434(1999)014<0326:AUSHIP>2.0.CO;2.

——, ——, and J. Baik, 1993: Upper-level eddy angular momentum flux and tropical cyclone intensity change. *J. Atmos. Sci.*, **50**, 1133–1147, https://doi.org/10.1175/1520-0469(1993)050<1133:ULEAMF>2.0.CO;2.

——, M. Mainelli, L. K. Shay, J. A. Knaff, and J. Kaplan, 2005: Further improvements to the Statistical Hurricane Intensity Prediction Scheme (SHIPS). *Wea. Forecasting*, **20**, 531–543, https://doi.org/10.1175/WAF862.1.

Ditchek, S. D., J. Molinari, K. L. Corbosiero, and R. G. Fovell, 2019: An objective climatology of tropical cyclone diurnal pulses in the Atlantic basin. *Mon. Wea. Rev.*, **147**, 591–605, https://doi.org/10.1175/MWR-D-18-0368.1.

Dudhia, J., 1989: Numerical study of convection observed during the winter monsoon experiment using a mesoscale two-dimensional model. *J. Atmos. Sci.*, **46**, 3077–3107, https://doi.org/10.1175/1520-0469(1989)046<3077:NSOCOD>2.0.CO;2.

Dunion, J. P., C. D. Thorncroft, and C. S. Velden, 2014: The tropical cyclone diurnal cycle of mature hurricanes. *Mon. Wea. Rev.*, **142**, 3900–3919, https://doi.org/10.1175/MWR-D-13-00191.1.

Fovell, R. G., Y. P. Bu, K. L. Corbosiero, W. Tung, Y. Cao, H. Kuo, L. Hsu, and H. Su, 2016: Influence of cloud microphysics and radiation on tropical cyclone structure and motion. *Multiscale Convection-Coupled Systems in the Tropics: A Tribute to Dr. Michio Yanai*, *Meteor. Monogr.*, No. 56, 11.1–11.27, https://doi.org/10.1175/AMSMONOGRAPHS-D-15-0006.1.

Gray, W. M., and R. W. Jacobson, 1977: Diurnal-variation of deep cumulus convection. *Mon. Wea. Rev.*, **105**, 1171–1188, https://doi.org/10.1175/1520-0493(1977)105<1171:DVODCC>2.0.CO;2.

Hobgood, J. S., 1986: A possible mechanism for the diurnal oscillations of tropical cyclones. *J. Atmos. Sci.*, **43**, 2901–2922, https://doi.org/10.1175/1520-0469(1986)043<2901:APMFTD>2.0.CO;2.

Hyndman, R. J., and G. Athanasopoulos, 2013: *Forecasting: Principles and Practice*. Open Access Books, http://otexts.org/fpp.

Jones, S. C., and Coauthors, 2003: The extratropical transition of tropical cyclones: Forecast challenges, current understanding, and future directions. *Wea. Forecasting*, **18**, 1052–1092, https://doi.org/10.1175/1520-0434(2003)018<1052:TETOTC>2.0.CO;2.

Kaplan, J., M. DeMaria, and J. A. Knaff, 2010: A revised tropical cyclone rapid intensification index for the Atlantic and east Pacific basins. *Wea. Forecasting*, **25**, 220–241, https://doi.org/10.1175/2009WAF2222280.1.

——, and Coauthors, 2015: Evaluating environmental impacts on tropical cyclone rapid intensification predictability utilizing statistical models. *Wea. Forecasting*, **30**, 1374–1396, https://doi.org/10.1175/WAF-D-15-0032.1.

Knaff, J. A., C. R. Sampson, and M. DeMaria, 2005: An operational statistical typhoon intensity prediction scheme for the western North Pacific. *Wea. Forecasting*, **20**, 688–699, https://doi.org/10.1175/WAF863.1.

——, S. P. Longmore, and D. A. Molenar, 2014: An objective satellite-based tropical cyclone size climatology. *J. Climate*, **27**, 455–476, https://doi.org/10.1175/JCLI-D-13-00096.1.

——, ——, R. T. Demaria, and D. A. Molenar, 2015: Improved tropical-cyclone flight-level wind estimates using routine infrared satellite reconnaissance. *J. Appl. Meteor. Climatol.*, **54**, 463–478, https://doi.org/10.1175/JAMC-D-14-0112.1.

——, C. R. Sampson, and G. Chirokova, 2017: A global statistical-dynamical tropical cyclone wind radii forecast scheme. *Wea. Forecasting*, **32**, 629–644, https://doi.org/10.1175/WAF-D-16-0168.1.

——, ——, and K. D. Musgrave, 2018: An operational rapid intensification prediction aid for the western North Pacific. *Wea. Forecasting*, **33**, 799–811, https://doi.org/10.1175/WAF-D-18-0012.1.

Kossin, J. P., 2002: Daily hurricane variability inferred from GOES infrared imagery. *Mon. Wea. Rev.*, **130**, 2260–2270, https://doi.org/10.1175/1520-0493(2002)130<2260:DHVIFG>2.0.CO;2.

Kraus, E. B., 1963: The diurnal precipitation change over the sea. *J. Atmos. Sci.*, **20**, 551–556, https://doi.org/10.1175/1520-0469(1963)020<0551:TDPCOT>2.0.CO;2.

Lajoie, F. A., and I. J. Butterworth, 1984: Oscillation of high-level cirrus and heavy precipitation around Australian region tropical cyclones. *Mon. Wea. Rev.*, **112**, 535–544, https://doi.org/10.1175/1520-0493(1984)112<0535:OOHLCA>2.0.CO;2.

Leith, C. E., 1973: Statistical problems of long-range forecasting. *Bull. Amer. Meteor. Soc.*, **54**, 266–266.

Leppert, K. D., and D. J. Cecil, 2016: Tropical cyclone diurnal cycle as observed by TRMM. *Mon. Wea. Rev.*, **144**, 2793–2808, https://doi.org/10.1175/MWR-D-15-0358.1.

McBride, J. L., and W. M. Gray, 1980: Mass divergence in tropical weather systems Paper II: Large-scale controls on convection. *Quart. J. Roy. Meteor. Soc.*, **106**, 517–538, https://doi.org/10.1002/qj.49710644909.

Melhauser, C., and F. Q. Zhang, 2014: Diurnal radiation cycle impact on the pregenesis environment of Hurricane Karl (2010). *J. Atmos. Sci.*, **71**, 1241–1259, https://doi.org/10.1175/JAS-D-13-0116.1.

Merritt, E. S., and R. Wexler, 1967: Cirrus canopies in tropical storms. *Mon. Wea. Rev.*, **95**, 111–120, https://doi.org/10.1175/1520-0493(1967)095<0111:CCITS>2.3.CO;2.

Miller, R. A., and W. M. Frank, 1993: Radiative forcing of simulated tropical cloud clusters. *Mon. Wea. Rev.*, **121**, 482–498, https://doi.org/10.1175/1520-0493(1993)121<0482:RFOSTC>2.0.CO;2.

Mueller, K. J., M. DeMaria, J. Knaff, J. P. Kossin, and T. H. Vonder Haar, 2006: Objective estimation of tropical cyclone wind structure from infrared satellite data. *Wea. Forecasting*, **21**, 990–1005, https://doi.org/10.1175/WAF955.1.

Muramatsu, T., 1983: Diurnal-variations of satellite-measured T_{bb} areal distribution and eye diameter of mature typhoons. *J. Meteor. Soc. Japan*, **61**, 77–90, https://doi.org/10.2151/jmsj1965.61.1_77.

Nicholls, M. E., 2015: An investigation of how radiation may cause accelerated rates of tropical cyclogenesis and diurnal cycles of convective activity. *Atmos. Chem. Phys.*, **15**, 9003–9029, https://doi.org/10.5194/acp-15-9003-2015.

O'Neill, M. E., D. Perez-Betancourt, and A. A. Wing, 2017: Accessible environments for diurnal-period waves in simulated tropical cyclones. *J. Atmos. Sci.*, **74**, 2489–2502, https://doi.org/10.1175/JAS-D-16-0294.1.

Pendergrass, A. G., and H. E. Willoughby, 2009: Diabatically induced secondary flows in tropical cyclones. Part I: Quasi-steady forcing. *Mon. Wea. Rev.*, **137**, 805–821, https://doi.org/10.1175/2008MWR2657.1.

Randall, D. A., Harshvardhan, and D. A. Dazlich, 1991: Diurnal variability of the hydrologic cycle in a general circulation model. *J. Atmos. Sci.*, **48**, 40–62, https://doi.org/10.1175/1520-0469(1991)048<0040:DVOTHC>2.0.CO;2.

Riehl, H., 1947: Diurnal variation of cloudiness over the subtropical Atlantic Ocean. *Bull. Amer. Meteor. Soc.*, **28**, 37–40, https://doi.org/10.1175/1520-0477-28.1.37.

Riemer, M., and F. Laliberte, 2015: Secondary circulation of tropical cyclones in vertical wind shear: Lagrangian diagnostic and pathways of environmental interaction. *J. Atmos. Sci.*, **72**, 3517–3536, https://doi.org/10.1175/JAS-D-14-0350.1.

Ruppert, J. H., Jr., and C. Hohenegger, 2018: Diurnal circulation adjustment and organized deep convection. *J. Climate*, **31**, 4899–4916, https://doi.org/10.1175/JCLI-D-17-0693.1.

Sampson, C. R., and A. J. Schrader, 2000: The Automated Tropical Cyclone Forecasting System (version 3.2). *Bull. Amer. Meteor. Soc.*, **81**, 1231–1240, https://doi.org/10.1175/1520-0477(2000)081<1231:TATCFS>2.3.CO;2.

Schubert, W. H., and J. J. Hack, 1982: Inertial stability and tropical cyclone development. *J. Atmos. Sci.*, **39**, 1687–1697, https://doi.org/10.1175/1520-0469(1982)039<1687:ISATCD>2.0.CO;2.

Shay, L. K., G. J. Goni, and P. G. Black, 2000: Effects of a warm oceanic feature on Hurricane Opal. *Mon. Wea. Rev.*, **128**, 1366–1383, https://doi.org/10.1175/1520-0493(2000)128<1366:EOAWOF>2.0.CO;2.

SHIPS, 2018: SHIPS statistical tropical cyclone intensity forecast technique development, developmental data. Accessed 15 August 2018, http://rammb.cira.colostate.edu/research/tropical_cyclones/ships/developmental_data.asp.

Silva Dias, P. L., J. P. Bonatti, and V. E. Kousky, 1987: Diurnally forced tropical tropospheric circulation over South America. *Mon. Wea. Rev.*, **115**, 1465–1478, https://doi.org/10.1175/1520-0493(1987)115<1465:DFTTCO>2.0.CO;2.

Steranka, J., E. B. Rodgers, and R. C. Gentry, 1984: The diurnal variation of Atlantic Ocean tropical cyclone cloud distribution inferred from geostationary satellite infrared measurements. *Mon. Wea. Rev.*, **112**, 2338–2344, https://doi.org/10.1175/1520-0493(1984)112<2338:TDVOAO>2.0.CO;2.

Student (William S. Gosset), 1908: The probable error of a mean. *Biometrika*, **6**, 1–25, https://doi.org/10.1093/biomet/6.1.1.

Tao, W. K., S. Lang, J. Simpson, C. H. Sui, B. Ferrier, and M. D. Chou, 1996: Mechanisms of cloud–radiation interaction in the tropics and midlatitudes. *J. Atmos. Sci.*, **53**, 2624–2651, https://doi.org/10.1175/1520-0469(1996)053<2624:MOCRII>2.0.CO;2.

Velden, C. S., and J. Sears, 2014: Computing deep-tropospheric vertical wind shear analyses for tropical cyclone applications: Does the methodology matter? *Wea. Forecasting*, **29**, 1169–1180, https://doi.org/10.1175/WAF-D-13-00147.1.

Vigh, J. L., J. A. Knaff, and W. H. Schubert, 2012: A climatology of hurricane eye formation. *Mon. Wea. Rev.*, **140**, 1405–1426, https://doi.org/10.1175/MWR-D-11-00108.1.

Weickmann, H. K., A. B. Long, and L. R. Hoxit, 1977: Some examples of rapidly growing oceanic cumulonimbus clouds. *Mon. Wea. Rev.*, **105**, 469–476, https://doi.org/10.1175/1520-0493(1977)105<0469:SEORGO>2.0.CO;2.

Wilks, D. S., 2006: *Statistical Methods in the Atmospheric Sciences*. 2nd ed. Elsevier, 627 pp.

Xu, K. M., and D. A. Randall, 1995: Impact of interactive radiative-transfer on the macroscopic behavior of cumulus ensembles. Part II: Mechanisms for cloud–radiation interactions. *J. Atmos. Sci.*, **52**, 800–817, https://doi.org/10.1175/1520-0469(1995)052<0800:IOIRTO>2.0.CO;2.

Yang, G. Y., and J. Slingo, 2001: The diurnal cycle in the tropics. *Mon. Wea. Rev.*, **129**, 784–801, https://doi.org/10.1175/1520-0493(2001)129<0784:TDCITT>2.0.CO;2.

Zehr, R. M., and J. A. Knaff, 2007: Atlantic major hurricanes, 1995–2005: Characteristics based on best-track, aircraft, and IR images. *J. Climate*, **20**, 5865–5888, https://doi.org/10.1175/2007JCLI1652.1.